

p-norms of histogram of oriented gradients for X-ray images

Nuha H. Hamada, Faten F. Kharbat

College of Engineering, Al Ain University, Abu Dhabi, United Arab Emirates

Article Info

Article history:

Received Jun 18, 2020

Revised Dec 8, 2020

Accepted Mar 22, 2021

Keywords:

Feature descriptor

HOG algorithm

Image classification

p-norms

X-ray images

ABSTRACT

Lebesgue spaces (L^p over R^n) play a significant role in mathematical analysis. They are widely used in machine learning and artificial intelligence to maximize performance or minimize error. The well-known histogram of oriented gradients (HOG) algorithm applies the 2-norm (Euclidean distance) to detect features in images. In this paper, we apply different *p*-norm values to identify the impact that changing these norms has on the original algorithm. The aim of this modification is to achieve better performance in classifying X-ray medical images related to of COVID-19 patients. The efficiency of the *p*-HOG algorithm is compared with the original HOG descriptor using a support vector machine implemented in Python. The results of the comparisons are promising, and the *p*-HOG algorithm shows greater efficiency in most cases.

This is an open access article under the [CC BY-SA](https://creativecommons.org/licenses/by-sa/4.0/) license.



Corresponding Author:

Nuha H. Hamada

College of Engineering

Al Ain University

United Arab Emirates

Email: nuha.hamada@aau.ac.ae

1. INTRODUCTION

The histogram of oriented gradients (HOG) is a well-known feature extraction algorithm used especially for human descriptors [1]. The HOG descriptor is based on the location and orientation of the edge. The literature has used HOG descriptors in conjunction with linear support vector machine (SVM) classifiers [2] and other data mining algorithms [1]. The strength of the HOG algorithm lies in its ability to capture edge and gradient information while decreasing the weight of irrelevant features due to illumination conditions [3]. However, many researchers have aimed to improve the HOG algorithm to enhance detection performance in terms of accuracy, computational costs, and classification. For example, the CoHOG [4] approach uses pairs of gradient orientations to form histograms. HOG-LBP, which was developed in [5] and [3], combines a local binary pattern (LBP) and HOG descriptor to produce better results. HOG was also enhanced by a complementary descriptor in the proposed eHOG algorithm [6] to handle the scale variation of pedestrians. In [7], the authors reduced the dimensions of the HOG features by combining HOG and greedy algorithms for selected HOG descriptors. Other work has also been conducted to enhance HOG features, including [8] and [9], among others.

HOG [2] is an effective feature descriptor technique that computes edge direction by dividing an image into blocks from which it extracts the histogram gradient information. The HOG feature descriptor, defined in [2], extracts useful information from a given image and discards extraneous information. In general, the HOG process contains three phases for the divided blocks, as described in [1]: i) conducting image normalization, ii) computing the image gradients for *x* and *y* directions, and iii) collecting HOG descriptors for all blocks. In the original algorithm proposed in [2], the Euclidean norm was utilized to calculate the gradient magnitude. Since *p*-norms are crucial in both pure and applied mathematics, other

norms can be used to calculate length or magnitude. In fact, L^p spaces (or Lebesgue spaces) have a key role in mathematical analysis and are used in many disciplines, such as computer science, engineering, physics, statistics, and finance [10]. The p -norm or L^p -norm of a vector $x = (x_1, x_2)$ in R^2 is defined as follows:

$$\|x\|_p = (|x_1|^p + |x_2|^p)^{1/p} \quad (1)$$

where p is a real number ≥ 1 . If $p = 1$ (called the L^1 norm), the distance between two points is the total distance traveled: $\|x\|_1 = |x_1| + |x_2|$. Thus, $p = 1$ counts the total changes in both x and y directions. If $p = 2$, we have the Euclidean norm (L^2 norm), i.e., the shortest distance between two points: $\|x\|_2 = \sqrt{x_1^2 + x_2^2}$. It is widely used and is the only norm invariant under any unitary transform, such as rotation. $p = \infty$ considers the highest gradient change and ignores the smallest one, where L^∞ norm of $x = (x_1, x_2)$ is defined as:

$$\|x\|_\infty = \max\{|x_1|, |x_2|\} \quad (2)$$

Given the power of p -norms in maximizing performance or minimizing error, it could be argued that the Euclidean norm (or 2-norm) in HOG descriptors is not necessarily the only choice for detecting the actual histogram gradient in an image. In reality, image scaling and resolution are known to affect the performance of feature detection. Different p -norms may enhance the capturing of actual distances for a suitable value of p . Different p -norm values are expected to affect the performance of the HOG feature detector in different ways.

In R^n , all norms are equivalent [10]—i.e., for any norm $\|x\|_p$ and $\|x\|_q$, there are positive constants c and k such that $c\|x\|_p \leq \|x\|_q \leq k\|x\|_p$ for all $x \in R^n$. In other words, there is only one norm topology in R^n . Consequently, the convergence of a sequence of vectors in R^n is independent of the choice of p -norm. Nevertheless, different norms offer flexibility to prove convergence. In numerical analysis, choosing a suitable norm plays a role in efficiently determining convergence. Convergence in infinite-dimensional vector spaces depends on the choice of p -norm, as p -norms in infinite-dimensional vector spaces are not equivalent [10]. Usually, one norm is more suitable than others for solving certain problems. For instance, the 1-norm (rather than the 2-norm) can be used to find the total distance traveled in a rectangular street grid from a location marked as the origin and the destination $point(x, y)$. In approximation theory, optimization problems depend on the choice of p -norm algorithm to obtain optimal solutions [11], [12]. In short, solutions to a problem can vary with different norms.

p -norms are widely used in machine learning and artificial intelligence and are powerful tools for evaluating and improving machine learning models. Prediction in machine learning relies on detecting patterns and inferences, rather than explicit instructions. Using sample data when building machine learning algorithms requires testing the predictive models to achieve the best performance. Maximizing the performance or minimizing the error of a model, in other words, aims to minimize the cost function. Norms are useful in measuring such errors [13]. In addition, solving an optimization problem means finding the input that best minimizes some output penalty [14]. Norms assign a magnitude to these outputs and hence enable penalties to be minimized.

In machine learning, different norms can be used for regularization and feature selection, as a loss function, and so on. Choosing which norm to use depends on the problem to be solved, as each norm has its own pros and cons [15]. The principle of parsimony in machine learning is commonly used to create a prediction model with good sparse approximation. Regularization techniques with different norms are applied to address overfitting, outliers, and feature selection in a model [13].

The L^1 norm is often used to calculate the Manhattan or taxicab distance, mean absolute error (MAE), and the least absolute shrinkage and selection operator (LASSO). LASSO uses L^1 regularization to reduce the huge number of features in a model by removing less important features, since L^1 is robust towards outliers and missing data [13]. On the other hand, the L^2 norm is often used to calculate Euclidean distance, mean squared error (MSE) and least squares error, and the ridge operator, which uses L^2 regularization to handle overfitting [13]. There are many efficient methods available for the widely used L^2 norm; however, the L^2 norm is sensitive to outliers due to enormous squared error values.

Moreover, extracting meaningful features requires robust feature selection methods that can eliminate noisy points. In [16] proposed joint $L^{1.2}$ norm minimization on both loss function and regularization to make feature selection more efficient. This idea reflects the effect of using more than one norm within one technique. Researchers have worked on improving the framework of SVMs (along with other algorithms) using p -norms. Some have proposed a 1-norm SVM to achieve more sparse classifiers [17]. Others have introduced a new approach using a $0 < p < 1$ norm [18], which was shown to be more effective than the 1-norm SVM.

In this paper, we investigate different p -norm values in the HOG algorithm (p -HOG) to achieve better performance in classifying medical X-ray images. To test different norms in the proposed modification, we used a dataset of X-ray images from COVID-19 patients and recorded the results of comparing the original HOG and p -HOG algorithms using different p -norm values. Both were implemented in Python. The paper is organized as follows. In section 2, we describe the steps of including the p -norm in the HOG algorithm and present the experiments performed on the dataset. We display and discuss the results in section 3, then conclude the paper in section 4.

2. RESEARCH METHOD

2.1. p -HOG algorithm

As mentioned in the introduction, p -norms are widely used in machine learning to improve predictive models. Using the p -norms with the best performance and accuracy will affect our findings. In this section, we propose the p -HOG algorithm by changing how we measure distance using different p -norms instead of the Euclidean norm. The goal is to improve the HOG descriptor's detection process. In the original HOG algorithm, it is necessary to extract the main feature descriptor to identify image features. The information in each $8\text{-pixel} \times 8\text{-pixel}$ cell is compacted to a nine-dimensional space consisting of nine angular bins which are equally divided over $0^0\text{--}180^0$ according to their gradient directions. The following steps explain the use of the p -norm in the algorithm. All steps except step 3 are derived from the HOG algorithm.

- Select the main block with a size ratio of 1:2.
- Divide the main block into $8\text{-pixel} \times 8\text{-pixel}$ cells to compute the histogram of gradients in x and y directions (denoted as g_x and g_y , respectively), as shown in Figure 1. Figure 1 illustrates the histogram generated for a single cell.

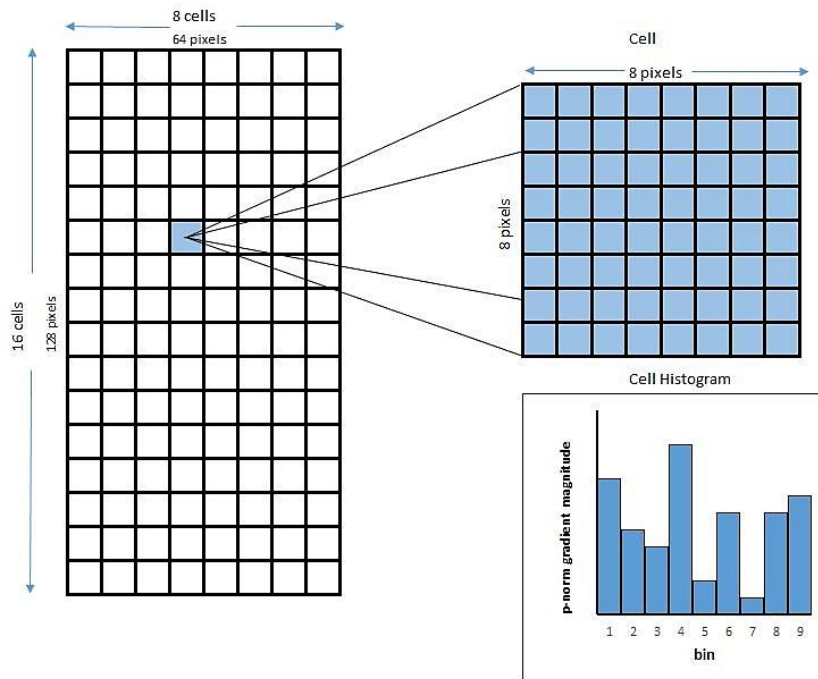


Figure 1. Histogram generated for a single cell

- Compute the L^p gradient magnitude, given as

$$||g||_p = (|g_x|^p + |g_y|^p)^{1/p} \quad (3)$$

where p is a real number ≥ 1 , and the L^p gradient direction angle by:

$$\tan^{-1} \frac{g_y}{g_x} \quad (4)$$

- Normalize the block of 16×16 pixels (or $4 = 2 \times 2$ cells) to reduce the variation of gradient magnitude that occurred by the shadows comes over a broad range. The resulting $4 \times 9 = 36$ -dimensional space histogram is normalized to unit length, as illustrated in Figure 2.

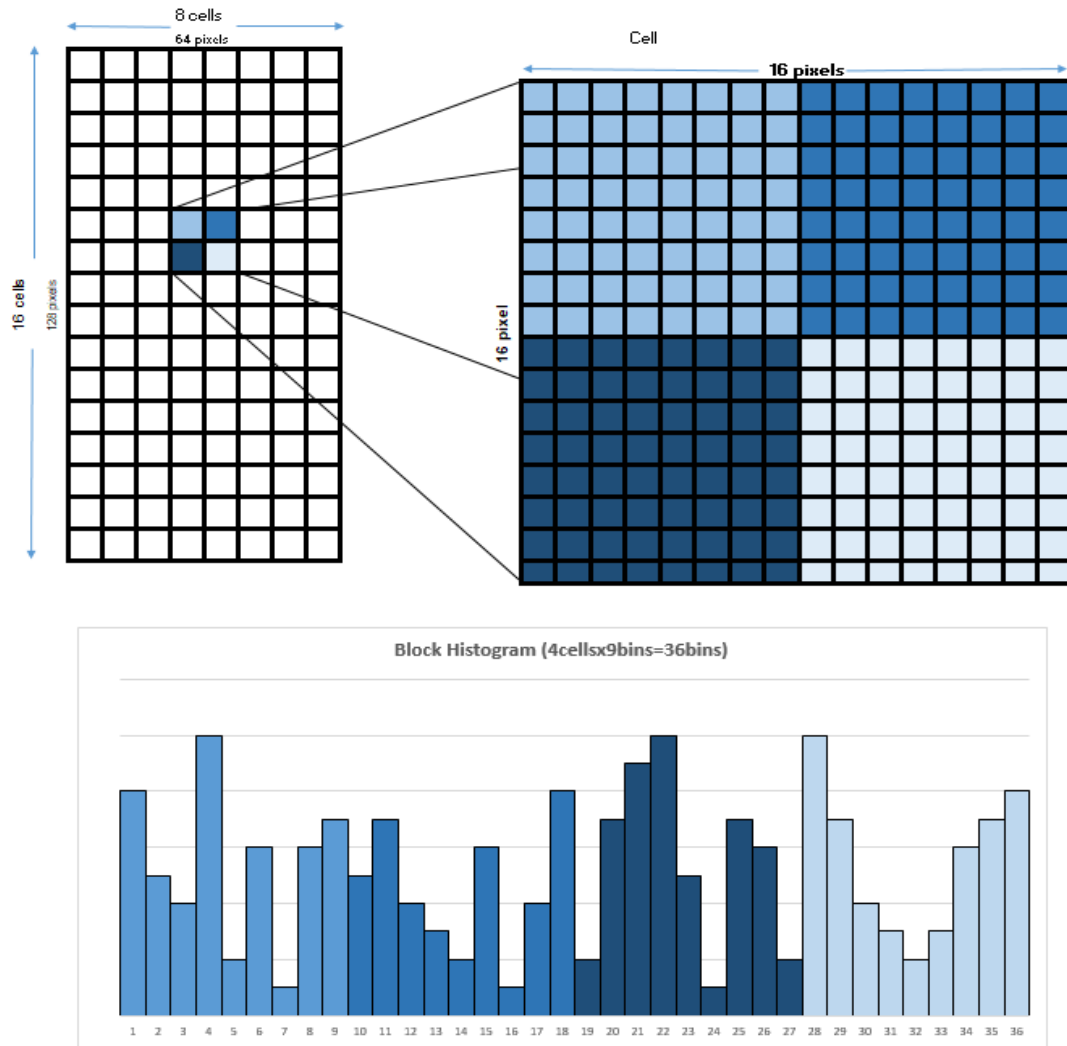


Figure 2. Histogram generated for a block of four cells

2.2. Experiments

Coronavirus disease 2019 (COVID-19) is a widespread disease caused by SARS-CoV-2 [19]. The disease first hit Wuhan, China, in late December 2019. As the number of confirmed cases increased rapidly, COVID-19 was declared a pandemic on March 11, 2020 [20]. COVID-19 can be diagnosed based on a combination of symptoms, including fever (87.9%), dry cough (67.7%), fatigue (38.0%), and sputum production (33.4%), among others [21]. On March 27, 2020, the World Health Organization (WHO) announced that the outbreak included 509,164 confirmed cases, which resulted in 23,335 deaths across 201 countries [22], [23] a death rate of approximately 4.6%. The growth in the number of diagnosed cases is due to close contact and human-to-human transmission [20], [24]. Scientists all over the world are working hard to overcome this health crisis, which poses a severe threat to public health especially to older patients with chronic diseases due to the unpredictable jump in COVID-19 patients. Chest X-rays can be used to detect the features of pneumonia [21], [24]; therefore, this research will conduct comparison experiments using a set of X-ray images.

2.2.1. Dataset selection

In general, datasets of COVID-19 X-ray images are still evolving. The dataset used in this paper included two categories, +COVID-19 and -COVID-19, which indicate scans of patients with and without COVID-19, respectively. The +COVID-19 X-ray images used in this research were collected by [25]. In the original data he provided, only positive COVID-19 cases were included. Other images related to SARS and MERS were ignored. The total images included 25 +COVID-19 images. The dataset used was relatively small; however, as these experiments were performed as a proof of concept and since this type of image is still not attainable at a large scale, this dataset is considered acceptable [26]. The -COVID-19 data was downloaded from [27], where images of pneumonia were collected and stored in the Kaggle repository. However, [28] collected 25 images from the repository to avoid noisy, mislabeled, and blurry images. In this research, we use the final data from [28].

2.2.3. Experimental setup

Python 3.7.3 was set up with the packages necessary such as skimage, numpy, and openCV to perform the experiments presented in this paper. The specifications of the computer system used were as follows: Intel® Core™ i7-8750 H CPU (3.70 GHz, 9 M Cache) and 16.00 GB RAM. We used 10-fold cross-validation to ensure more reliable results from the generated models.

For each image, both the original HOG and the p -HOG feature detector descriptors are applied. The original HOG descriptor was extracted from the original Python implementation in the sklearn package, which depends on the scale-invariant feature transform (SIFT) algorithm [29]. The p -HOG implementation was based on the implementation found in [30]. The modifications were implemented in the methods, adding the “norm” parameter for the magnitude method and using the new value to find the orientation, gradient, and HOG calculations.

The generated HOG and p -HOG descriptors for all images were fed separately into the SVM algorithm to generate a different model for each, which was later used in classification. The model was evaluated using the unseen testing set, and the results were recorded and compared. To generate a full picture of the p -norm's effect on the results, different p -norm values were tested: p -norm = 1, 2, 10, 20, and ∞ . Moreover, 10-fold cross-validation was used to ensure the reliability of the produced results, and a t -test was used to record whether the differences between results were statistically significant.

2.2.3. Performance measures

Different tools are used to compare results of different data mining algorithms [31]. One such tool is the confusion matrix, which is used as “an indication of the properties of a classification (discriminant) rule” [31]. The confusion matrix has four values that indicate the number of cases correctly and incorrectly classified for each class. In this research, there are two classes: +COVID-19 and -COVID-19. The true positive (TP) rate refers to the correct classification of the positive cases, and the false positive (FP) rate indicates the incorrect classification of positive cases as negative. The true negative (TN) rate describes the correct classification of normal cases, and the false negative (FN) rate represents the incorrect classification of normal cases. Although accuracy is not the only indicator used, it can be considered one of the most important. Accuracy is computed using (5). Another indication is recall or sensitivity, which shows how well the positive cases is calculated using (6) [31].

$$accuracy = \frac{TP+TN}{TP+FP+TN+FN} \quad (5)$$

$$recall/sensitivity = \frac{TP}{TP+FN} \quad (6)$$

Precision shows how many positively classified cases were relevant. High precision indicates that cases labeled as positive were indeed positive, with a very small number of FPs. Specificity is another useful indicator that describes the number of cases without the disease who test negative [31].

$$precision = \frac{TP}{TP+FP} \quad (7)$$

$$specificity = \frac{TN}{TN+FP} \quad (8)$$

Finally, the F -measure combines precision and recall to ensure that they are balanced. The calculating for the F -measure is being as [31]:

$$F - measure = \frac{2 * recall * precision}{recall + precision} \quad (9)$$

3. RESULTS AND DISCUSSION

The results in Table 1 reveal that using the linear kernel with the original HOG algorithm resulted in 94.8% accuracy and precision and recall values of 97% and 91.8%, respectively. Using the p -HOG algorithm (with any norm value) increased accuracy to 95% (L^2 , L^∞) or 96% (L^1). To ensure that the differences were statistically significant, a t -test was conducted between the original HOG and p -HOG results. The t -test showed significant differences ($p < 0.1$) in precision, recall, and specificity ($p = 0.03$, $p = 0.08$, and $p = 0.03$, respectively). Although accuracy was not significantly different, the improvements in recall and specificity seem to indicate a good influence on p -HOG. Another step was taken to further explore the recorded results—that is, to compare the norm values in the p -HOG implementation. In terms of recall and accuracy, L^1 had significantly better results than the other norm values ($norm=2$ and $norm=10$, respectively).

Table 1. The results of SVM with linear kernel using HOG and p -HOG with different norms

Linear Kernel	Norm	Precision	Recall	F-measure	Specificity	Accuracy
p -HOG	1	99.0%	93.8%	96.3%	99.0%	96.0%
	2	99.0%	89.6%	94.1%	99.0%	95.0%
	10	100.0%	91.7%	95.6%	100.0%	95.5%
	20	100.0%	91.7%	95.7%	100.0%	95.0%
	∞	100.0%	88.3%	93.8%	100.0%	95.0%
HOG		97.6%	91.8%	94.6%	97.8%	94.8%

The results in Table 2 reveal that using the RBF kernel with the original HOG algorithm resulted in 95.2% accuracy. These results were very similar to the p -HOG results using different norm values, with the exception of the L^1 result, which was high at 97.0%. The difference in accuracy is also reflected in the recall, F -measure, and specificity scores, where the p -HOG (L^1) results surpass (with statistical significance) the results of the original HOG algorithm and those of the p -HOG algorithm with other norm values. Again, L^1 showed better results than any other norm values and the original HOG algorithm, stressing the same conclusion as before.

Table 2. The results of SVM with RBF kernel using HOG and p -HOG with different norms

RBF Kernel	Norm	Precision	Recall	F-measure	Specificity	Accuracy
p -HOG	1	100.0%	93.1%	96.4%	100.0%	97.0%
	2	98.0%	91.0%	94.4%	98.0%	94.5%
	10	100.0%	91.7%	95.7%	100.0%	95.5%
	20	100.0%	89.7%	94.6%	100.0%	95.0%
	∞	100.0%	89.8%	94.6%	100.0%	95.0%
HOG		98.6%	91.7%	95.0%	98.4%	95.2%

Finally, in Table 3, the results using the sigmoid kernel showed better results in general for p -HOG over the original HOG. However, based on the t -test results, the differences are not statistically significant except for the recall value, where p -HOG shows statistically significant improvement. In general, exploring different p -norm values enhanced the SVM's performance in classifying images. This result reveals that using p -HOG with L^1 to detect +COVID-19 X-ray images is promising. Our results stress that L^1 is robust towards outliers and consequently achieves better results in detecting +COVID-19 X-ray images. Detecting edges in X-rays occurs when colors change from white to black (or gray), or vice versa, which thus has a large gradient magnitude compared with changing colors gradually.

Table 3. The results of SVM with sigmoid kernel using HOG and p -HOG with different norms

sigmoid Kernel	Norm	Precision	Recall	F-measure	Specificity	Accuracy
p -HOG	1	100.0%	92.4%	96.1%	100.0%	96.0%
	2	98.0%	91.8%	94.8%	98.0%	95.0%
	10	100.0%	92.8%	96.2%	100.0%	95.5%
	20	100.0%	90.3%	94.9%	100.0%	95.0%
	∞	100.0%	90.2%	94.8%	100.0%	95.5%
HOG		98.8%	91.8%	95.1%	98.8%	95.1%

4. CONCLUSION

In this paper, we proposed p -HOG feature detection. The main idea of p -HOG is to apply different norm values when calculating gradient magnitude. Gradient computation detector performance is sensitive to how gradients are computed. Different p -norms were tested on X-ray images of COVID-19 cases. Our experimental results show that the performance of the p -HOG descriptor was significantly higher than the HOG descriptor in terms of precision, accuracy, and specificity, regardless of SVM kernel. The L^1 norm shows the best results, emphasizing the robustness of this norm and its resistance to outliers in X-ray images, which mainly include the colors white, black, and gray. However, one of our limitations in this research was small sample size due to restrictions on releasing COVID-19 data. In future work, we intend to investigate the effectiveness of p -HOG for detecting other chest diseases in X-ray images.

REFERENCES

- [1] F. F. Kharbat, T. Elamsy, A. Mahmoud and R. Abdullah, "Image Feature Detectors for Deepfake Video Detection," *2019 IEEE/ACS 16th International Conference on Computer Systems and Applications (AICCSA)*, Abu Dhabi, United Arab Emirates, 2019, pp. 1-4, doi: 10.1109/AICCSA47632.2019.9035360.
- [2] N. Dalal and B. Triggs, "Histograms of oriented gradients for human detection," *2005 IEEE Computer Society Conference on Computer Vision and Pattern Recognition (CVPR'05)*, San Diego, CA, USA, vol. 1, 2005, pp. 886-893, doi: 10.1109/CVPR.2005.177.
- [3] M. Ghorbani, A. T. Targhi and M. M. Dehshibi, "HOG and LBP: Towards a robust face recognition system," *2015 Tenth International Conference on Digital Information Management (ICDIM)*, Jeju, Korea (South), 2015, pp. 138-141, doi: 10.1109/ICDIM.2015.7381860.
- [4] T. Watanabe, S. Ito, and K. Yokoi, "Co-occurrence Histograms of Oriented Gradients for Pedestrian Detection," in *Advances in Image and Video Technology*, pp. 37-47, 2009, doi: 10.1007/978-3-540-92957-4_4.
- [5] X. Wang, T. X. Han and S. Yan, "An HOG-LBP human detector with partial occlusion handling," *2009 IEEE 12th International Conference on Computer Vision*, Kyoto, Japan, 2009, pp. 32-39, doi: 10.1109/ICCV.2009.5459207.
- [6] Y. Zhao, Y. Zhang, R. Cheng, D. Wei and G. Li, "An Enhanced Histogram of Oriented Gradients for Pedestrian Detection," in *IEEE Intelligent Transportation Systems Magazine*, vol. 7, no. 3, pp. 29-38, Fall 2015, doi: 10.1109/MITS.2015.2427366.
- [7] Y. Choi, S. Jeong, and M. Lee, "Feature Selection for HOG Descriptor Based on Greedy Algorithm," in *Neural Information Processing. ICONIP 2013. Lecture Notes in Computer Science*, vol. 8228, pp. 417-424, 2013, doi: 10.1007/978-3-642-42051-1_52.
- [8] R. P. Yadav, V. Senthilarasu, K. Kutty, and S. P. Ugale, "Implementation of robust HOG-SVM based pedestrian classification," *International Journal of Computer Applications*, vol. 114, no. 19, pp. 10-16, 2015, doi: 10.5120/20084-2026.
- [9] Y. Liu, J. Yao, R. Xie and S. Zhu, "Pedestrian detection from still images based on multi-feature covariances," *2013 IEEE International Conference on Information and Automation (ICIA)*, Yinchuan, China, 2013, pp. 614-619, doi: 10.1109/ICInfA.2013.6720370.
- [10] W. Rudin, "Functional analysis. 1991," *Internat. Ser. Pure Appl. Math*, 1991.
- [11] I. Singer, "Best approximation in normed linear spaces by elements of linear subspaces," New York, 1970.
- [12] G. Belitskii and others, "Matrix norms and their applications," Birkhäuser verlag basel, 1988.
- [13] S. Sra, S. Nowozin, and S. J. Wright, "Optimization for machine learning," Cambridge, Mit Press, 2012.
- [14] S. B. Kotsiantis, I. D. Zaharakis, and P. E. Pintelas, "Machine learning: a review of classification and combining techniques," *Artificial Intelligence Review.*, vol. 26, no. 3, pp. 159-190, 2006, doi: 10.1007/s10462-007-9052-3.
- [15] I. Goodfellow, Y. Bengio, and A. Courville, "Deep Learning," MIT Press, 2016.
- [16] F. Nie, H. Huang, X. Cai, and C. H. Ding, "Efficient and robust feature selection via joint ℓ_2 , 1-norms minimization," in *Advances in neural information processing systems*, vol. 23, pp. 1813-1821, 2010.
- [17] P. S. Bradley and O. L. Mangasarian, "Feature selection via concave minimization and support vector machines," in *ICML*, vol. 98, pp. 82-90, 1998.
- [18] J.-Y. Tan, C.-H. Zhang, and N.-Y. Deng, "Cancer related gene identification via p -norm support vector machine," in *The 4th international conference on computational systems biology*, vol. 1, pp. 101-108, 2010.
- [19] W. H. Organization and others, "Naming the coronavirus disease (COVID-19) and the virus that causes it," 2020.
- [20] Y. Zhou *et al.*, "Clinical reports on early diagnosis of novel coronavirus (2019-nCoV) pneumonia in stealth infected patients," *Preprints*, vol. 1, pp. 1-8, 2020, doi: 10.20944/preprints202002.0156.v1.
- [21] C. Sohrabi *et al.*, "World Health Organization declares global emergency: A review of the 2019 novel coronavirus (COVID-19)," *International Journal of Surgery*, vol. 76, pp. 71-76, Apr. 2020, doi: 10.1016/j.ijsu.2020.02.034.
- [22] W. H. O. WHO, "WHO Director-General's opening remarks at the media briefing on COVID-19 - 11 March 2020," 2020, [Online]. Available: <https://www.who.int/director-general/speeches/detail/who-director-general-s-opening-remarks-at-the-media-briefing-on-covid-19---11-march-2020>.
- [23] "COVID-19 Coronavirus Pandemic," *worldometers*, 2020. [Online]. Available: <https://www.worldometers.info/coronavirus/>.
- [24] Q. Han, Q. Lin, S. Jin, and L. You, "Coronavirus 2019-nCoV: A brief perspective from the front line," *Journal of Infection*, vol. 80, no. 4, pp. 373-377, Apr. 2020, doi: 10.1016/j.jinf.2020.02.010.
- [25] J. Cohen., "Covid chest x-ray dataset," 2020. [Online]. Available: <https://github.com/ieee8023/covid-%0Achestxray-dataset>.

- [26] S. Feng, H. Zhou, and H. Dong, "Using deep neural network with small dataset to predict material defects," *Materials & Design*, vol. 162, pp. 300-310, Jan. 2019, doi: 10.1016/j.matdes.2018.11.060.
- [27] P. Mooney, "Chest x-ray images (pneumonia)," *kaggle*, 2018.
- [28] A. Rosebrock, "Detecting COVID-19 in X-ray images with Keras, TensorFlow, and Deep Learning," [Online]. Available: <https://www.pyimagesearch.com/2020/03/16/detecting-covid-19-in-x-ray-images-with-keras-tensorflow-and-deep-learning>.
- [29] G. Lowe, "SIFT-the scale invariant feature transform," *International Journal*, vol. 2, pp. 91-110, 2004.
- [30] J. Kossaifi, "Vectorised implementation of the histogram of oriented gradients," 2020. [Online]. Available: <https://github.com/JeanKossaifi/python-hog>.
- [31] N. V. Chawla, "Data Mining for Imbalanced Datasets: An Overview," in *Data Mining and Knowledge Discovery Handbook*, Boston, MA: Springer US, 2009, pp. 875-886, doi: 10.1007/978-0-387-09823-4_45

BIOGRAPHIES OF AUTHORS



Nuha H. Hamada is an assistant professor working at Al Ain University, Abu Dhabi, UAE. She has completed her Ph.D. on Functional Analysis-Hilbert spaces from University of Baghdad. Her Ph.D. thesis addressed the Jordan *-derivation on the algebra of all bounded linear operators on separable infinite dimensional complex Hilbert space. Her research interests include supercyclic operators, cyclic phenomena and Chaos Theory. In addition, she has a contribution on the area of quantitative analysis in management, chaos theory from decision-making perspective, applying statistical technique to investigate difficulties in learning and find some cultural factors that affect the process of teaching and learning and studying how LMS can support teaching and learning.



Faten F. Kharbat holds PhD degree in Computer Science: Data Mining and Knowledge Discovery from the University of the West of England, UK. Her MSc and BSc were in Computer Science from University of Jordan. Her main research interest is Cancer care Informatics, health informatics, image processing, content analysis, applied data mining, and recently was involved in quality of higher education. She is an Associate Professor in Computer Science at Al Ain University, Abu Dhabi Campus, UAE. At the moment, she is the deputy dean for the College of Engineering in Abu Dhabi Campus.